ACS OMEGA

http://pubs.acs.org/journal/acsodf

Article

Shedding Light on the Synthesis, Crystal Structure, Characterization, and Computational Study of Optoelectronic Properties and Bioactivity of Imine derivatives

Muhammad Ashfaq,* Muhammad Nawaz Tahir, Shabbir Muhammad, Khurram Shahzad Munawar,* Saqib Ali, Gulzar Ahmed, Abdullah G. Al-Sehemi, Saleh S. Alarfaji, and Muhammad Ehtisham Ibraheem Khan

Cite This: *ACS Omega* 2022, 7, 5217−5230

Read Online

ACCESS | Metrics & More | Article Recommendations | Supporting Information

ABSTRACT: Two imine compounds named as (*E*)-2-(((3,4-dichlorophenyl)imino)methyl)phenol (**DC2H**) and (*E*)-4-(((2,4-dimethylphenyl)imino)methyl)phenol (**DM4H**) are synthesized, and their crystal structures are verified using the single-crystal X-ray diffraction (XRD) technique. The crystal structures of the compounds are compared with the closely related crystal structures using the Cambridge Structural Database (CSD). The crystal packing in terms of intermolecular interactions is fully explored by Hirshfeld surface analysis. Void analysis is carried out for both compounds to check the strength of the crystal packing. Furthermore, a state-of-the-art dual computational technique consisting of quantum chemical and molecular docking methods is used to shed light on the molecular structure, optoelectronic properties, and bioactivity of indigenously synthesized compounds. The optimized molecular geometries are compared with their counterpart experimental values. Based on previous reports of biofunctions of the indigenously synthesized imine derivatives, they are explored for their potential inhibition properties against two very crucial proteins (main protease (M^{pro}) and nonstructural protein 9 (NSP9)) of SARS-CoV-2. The calculated interaction energy values of **DC2H** and **DM4H** with M^{pro} are found to be −6.3 and −6.6 kcal/mol, respectively, and for NSP9, the calculated interaction energy value is found to be −6.5 kcal/mol. We believe that the current combined study through experiments and computational techniques will not only pique the interest of the broad scientific community but also evoke interest in their further *in vitro* and *in vivo* investigations.

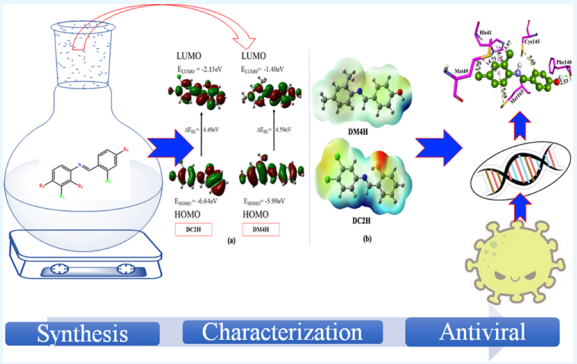

1. INTRODUCTION

Schiff bases belong to an important class of ligands bearing an imine or azomethine (−C═N−) functional group. Hugo Schiff, a German scientist and Nobel Prize laureate, prepared the first of these condensation products from primary amines and carbonyl compounds in 1864.[1,2] The Schiff base is a structural counterpart of a ketone or aldehyde that has had the carbonyl group (C═O) replaced with an imine or azomethine group.[3] Schiff bases are very vital due to their ease of synthesis, availability, and electrical characteristics, particularly in the synthesis of metal complexes *via* azomethine nitrogen.[4,5] Schiff base coordination chemistry has gotten a lot of interest because of its important functions in analytical chemistry, metal refining, organic synthesis, metallurgy, electroplating, and photography.[6,7] Schiff bases not only play an important role in advanced coordination chemistry but also are equally significant in bioinorganic chemistry.[8] They have a wide range of medical uses due to their pharmacological characteristics because of the presence of an azomethine (C═N) linkage.[9] As a result, antibacterial, anticancer, antifungal, and diuretic properties have been described for many azomethines.[10,11]

In addition to this, Schiff bases have a wide range of uses in the food and dye industries and also in catalysis and agrochemical activities.[12] The relevance of metal complexes of Schiff bases in catalysis, supramolecular chemistry, separation and encapsulation processes, materials science, biological applications, and the creation of molecules with unique characteristics and molecular structures has long been recognized.[13] The azomethine nitrogen of Schiff bases offers a binding site for metal ions to be linked to different biomolecules such as proteins and amino acids for antigerm actions in biological systems.[14] Various studies have shown

Received: November 9, 2021
Accepted: January 24, 2022
Published: February 2, 2022

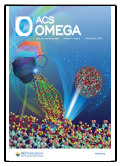

Table 1. SC-XRD Experimental Details of DC2H and DM4H

crystal data	DC2H	DM4H
CCDC	2102191	2102192
chemical formula	$C_{13}H_9Cl_2NO$	$C_{15}H_{15}NO$
M_r	266.11	225.28
crystal system, space group	orthorhombic, $P2_12_12_1$	orthorhombic, $Pca2_1$
temperature (K)	296	296
a, b, c (Å)	3.8954 (5), 11.0570 (13), 26.799 (4)	10.631 (2), 13.873 (3), 8.6997 (15)
α, β, γ (deg)	90, 90, 90	90, 90, 90
V (Å^3)	1154.3 (3)	1283.1 (4)
Z	4	4
density (calculated) g/cm^{-3}	1.531	1.166
F(000)	544	480
radiation type	Mo Kα	Mo Kα
wavelength (λ)	0.71073 Å	0.71073 Å
μ (mm^{-1})	0.542	0.073
crystal size (mm)	0.40 × 0.20 × 0.15	0.42 × 0.24 × 0.22
	Data Collection	
diffractometer	Bruker APEXII CCD diffractometer	Bruker APEXII CCD diffractometer
absorption correction	multiscan (SADABS; Bruker, 2007)	multiscan (SADABS; Bruker, 2007)
no. of measured, independent, and observed [$I > 2\sigma(I)$] reflections	10 413, 2760, and 1827	10 600, 1684, and 938
R_{int}	0.047	0.053
theta range for data collection (deg)	0.994−27.984	2.414−28.277
index ranges	$-4 \leq h \leq 5$, $-12 \leq k \leq 14$, and $-33 \leq l \leq 35$	$-13 \leq h \leq 13$, $-18 \leq k \leq 16$, and $-11 \leq l \leq 11$
$(\sin\theta/\lambda)_{max}$ (Å^{-1})	0.660	0.667
	Data Refinement	
$R[F^2 > 2\sigma(F^2)]$, $wR(F^2)$, S	0.043, 0.083, 0.97	0.054, 0.136, 1.00
no. of reflections	2760	1684
no. of parameters	155	157
H-atom treatment	H-atom parameters constrained	H atoms treated by a mixture of independent and constrained refinement
$\Delta\rho_{max}$, $\Delta\rho_{min}$ (e Å^{-3})	0.19, −0.23	0.19, −0.15

the enhanced biofunctionalities of Schiff bases as compared to their metal complexes. Depending on the transition metal ions present in Schiff bases, they exhibit antibacterial, antifungal, antiviral, antiulcer, and anticancer properties.[15,16] Using ring closure, cycloaddition, and replacement processes, Schiff bases have been used as synthons in the creation of a variety of commercial and physiologically active chemicals such as formazans, 4-thiazolidinines, benzoxazines, and so on.[17,18] The use of Schiff base derivatives in a variety of processes prompted researchers to create new Schiff bases for the development of environmentally friendly technologies.[19] Hirshfeld surface analysis[20] is an excellent way to explore the noncovalent interactions that are the key feature of the crystal packing of molecules in the solid state. We explore Hirshfeld surface analysis for **DC2H** and **DM4H**. Therefore, in continuation of our previous studies on Schiff bases and their metal complexes,[21−23] this time, we are reporting a completely experimental and computational study of two new Schiff bases named as **DC2H** and **DM4H**. A triple hybrid technique consisting of experimental, quantum chemical, and molecular docking methods will be used to investigate the above-synthesized molecules. The quantum chemical methods provide several fundamental insights into the structure−property relationship, which are incomprehensive with simple characterization techniques. Similarly, an in silico study through molecular docking highlights the potential of the studied ligands for their possible use as bioactive compounds against certain diseases, which we will assess for the inhibition of SARS-Co-V-2 in the current investigation.

2. RESULTS AND DISCUSSION

The Cambridge Structural Database (CSD) search confirms that the crystal structures of the tilted compounds are new. Moreover, a CSD search is performed to find the crystal structures that are closely related to our crystal structure. The closely related crystal structures are compared with the crystal structures of the titled compounds in terms of molecular configuration and crystal packing. Table 1 provides complete SC-XRD details of the titled compounds, whereas Table 2 provides a comparison of selected bond lengths and bond angles of the titled compounds.

2.1. SC-XRD Description of the Crystal Structure of DC2H and DM4H. In **DC2H** (Figure 1a, Table 1), o-cresol group A (C1-C7/O1) and 3,4-dichloroaniline group B (C8-C13/N1/Cl1/Cl2) are oriented at the dihedral angle of 6.8 (9)° with respect to each other, which indicates that the whole molecule is almost planar. The titled compound adopts a phenolic tautomeric form instead of a keto tautomeric form, as evident from the O1−C1 bond length of 1.360 (4) Å and the N1−C7 bond length of 1.278 (4) Å. Important bond lengths and bond angles of the titled compounds are given in Table 2. The molecular configuration is stabilized by the presence of intramolecular H-bonding of type O-H···N to form an S (6) H-bonded loop. The molecules are interlinked by the weak H-bonding of type C-H···Cl to form an infinite C12 zigzag chain that runs along the c crystallographic axis (Figure 2, Table S1). The neighboring chains are interlinked by a comparatively weak interaction of the off-set $\pi\cdots\pi$ stacking type. Phenyl rings (C1−C6) of symmetry-related

https://doi.org/10.1021/acsomega.1c06325
ACS Omega 2022, 7, 5217−5230

Table 2. Selected Bond Lengths (Å) and Bond Angles (deg) in DC2H and DM4H

selected bond lengths in **DC2H**		selected bond lengths in **DM4H**	
O1-C1	1.360 (4)	O1-C13	1.352 (4)
N1-C7	1.278 (4)	N1-C1	1.432 (5)
N1-C8	1.409 (4)	N1-C9	1.267 (5)
C6-C7	1.440 (4)	C9-C10	1.453 (5)
Cl1-C10	1.729 (3)	C2-C7	1.513 (6)
Cl2-C11	1.726 (3)	C4-C8	1.514 (6)
selected bond angles in **DC2H**		selected bond angles in **DM4H**	
O1-C1-C2	118.1 (3)	O1-C13-C12	117.4 (4)
O1-C1-C6	121.3 (3)	O1-C13-C14	122.7 (4)
C6-C7-N1	122.7 (3)	C10-C9-N1	126.3 (4)
C7-N1-C8	121.6 (3)	C9-N1-C1	117.1 (3)
N1-C8-C9	116.1 (3)	N1-C1-C2	120.0 (4)
C9-C10-Cl1	118.9 (3)	C1-C2-C7	122.1 (4)
C10-C11-Cl2	121.4 (3)	C3-C4-C8	121.2 (5)

molecules (x + 1, y, z) are involved in the off-set $\pi\cdots\pi$ stacking interaction with an intercentroid distance of 3.895 Å and a ring off-set value of 1.610 Å (Figure 3). Phenyl rings (C8−C13) of symmetry-related molecules (x + 1, y, z) are involved in the off-set $\pi\cdots\pi$ stacking interaction with an intercentroid distance of 3.895 Å and a ring off-set value of 1.805 Å. A Cambridge Structural Database search provides a lot of crystal structures related to **DC2H**. The two most closely related crystal structures are found in the database with reference codes **AWUSIV**[24] and **BANGOM03**,[25] which are compared with the crystal structure of the titled compound. Both **AWUSIV** and **BANGOM03** have one hydroxyl-substituted phenyl ring, while another phenyl ring in **AWUSIV** is trichloro-substituted, whereas in **BANGOM03**, another phenyl ring is pentafluoro-substituted. Like in **DC2H**, the molecular configuration of **AWUSIV** and **BANGOM03** is also stabilized by intramolecular H-bonding of type O-H···N. The whole molecule of **BANGOM03** is almost planar like the molecule of **DC2H**, but the molecule of **AWUSIV** is not planar as the dihedral angle between phenyl rings is 24.64 (11)°. The crystal packing of **DC2H** is different from the crystal packing of **AWUSIV** and **BANGOM03**. The crystal packing of **DC2H** is stabilized by C-H···O and off-set $\pi\cdots\pi$ stacking interactions, whereas the crystal packing of **BANGOM03** is stabilized by O-H···O and off-set $\pi\cdots\pi$ stacking interactions. No significant intermolecular H-bonding is present in the crystal packing of **AWUSIV**.

In **DM4H** (Figure 1b, Table 1), p-cresol group A (C9-C15/O1) and 2,4-dimethylaniline group B (C1-C7/N1) are oriented at a dihedral angle of 72.4 (8)° with respect to each other. The important bond lengths and bond angles of the titled compound are given in Table 2. The molecular configuration is stabilized by the presence of intramolecular H-bonding of type C-H···N to form an S (5) H-bonded loop. The molecules are interlinked by a strong O-H···N bonding to form a C8 zigzag chain that runs along the crystallographic a-axis, as given in Table S1 and shown in Figure 4. A comparatively weak H-bonding of type C-H···O is found in the crystal packing that interlinks the molecules in such a way that an infinite C5 chain is formed that runs along the c crystallographic axis, where CH is from the phenyl ring (C10−C15). No other type of weak intermolecular interaction is found in the crystal packing. A Cambridge Structural Database search provides two crystal structures that are most closely related to the crystal structure of the titled compound that contains one 4-hydroxyl-substituted phenyl ring, while the substitution on the other phenyl ring is different from the dimethyl-substituted phenyl ring in **DM4H**. Reference codes are **SECXAB**[26] (with one methyl

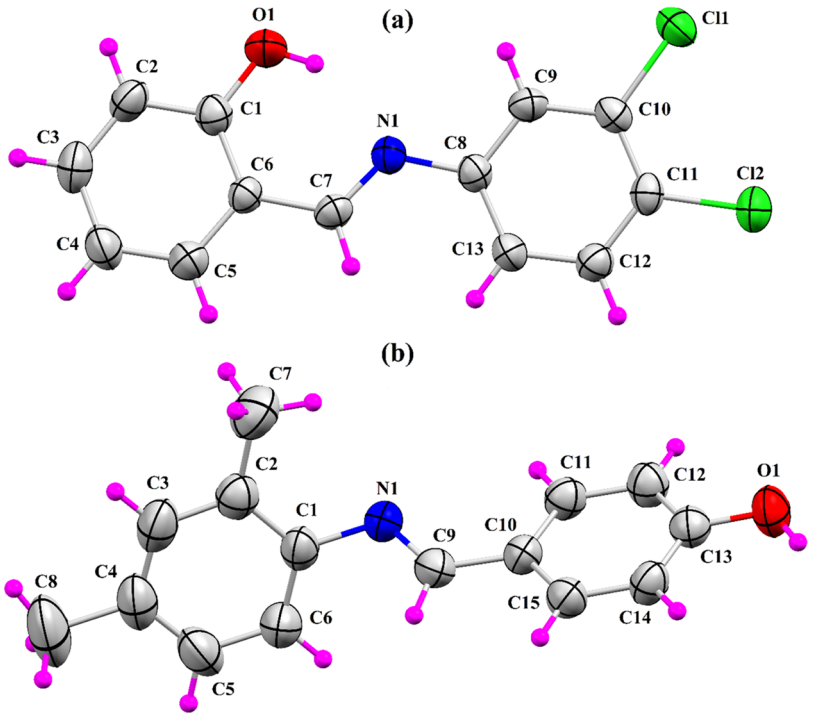

Figure 1. ORTEP diagram of (a) **DC2H** and (b) **DM4H**. The diagrams are drawn at a probability level of 50%. H-atoms are shown by small circles of arbitrary radii.

https://doi.org/10.1021/acsomega.1c06325
ACS Omega 2022, 7, 5217−5230

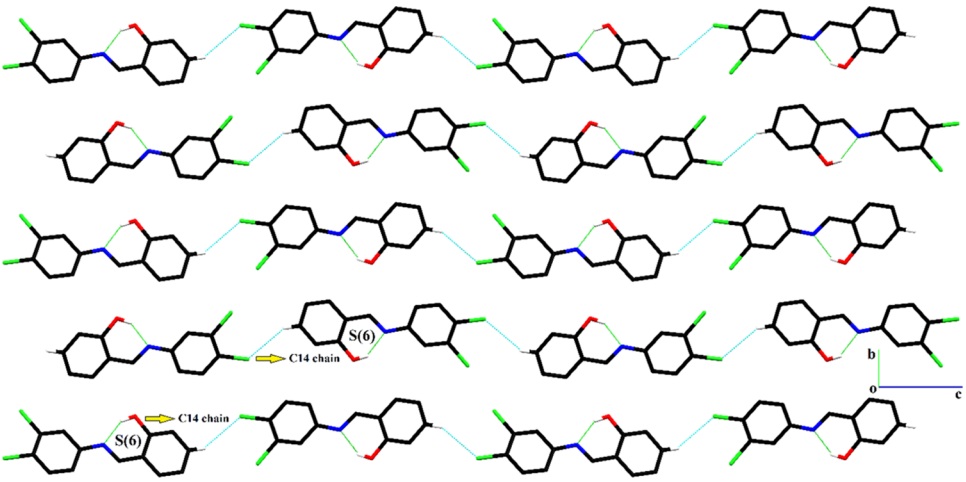

Figure 2. Packing diagram of **DC2H** shows that the molecules form infinite C14 chains that run along the c crystallographic axis. Only selected H-atoms are shown for clarity.

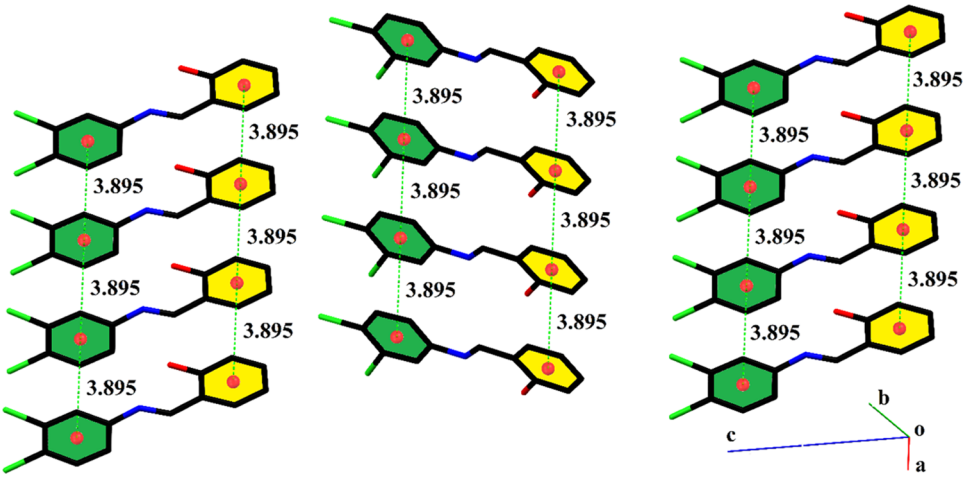

Figure 3. Graphical representation of the off-set $\pi\cdots\pi$ stacking interaction in the crystal packing of **DC2H**. H-atoms are not shown for clarity. Distances shown are measured in Å.

and chloro-substituted phenyl ring) and **TAMYOY**[27] (with one methyl-substituted phenyl ring). **DM4H** is different from **SECXAB** and **TAMYOY** in terms of stabilization of the molecular configuration because the molecular configuration of **DM4H** is stabilized by intramolecular H-bonding of type C-H···N, whereas in **SECXAB** and **TAMYOY**, no intramolecular H-bonding is present. Like **DM4H**, the molecules of **SECXAB** and **TAMYOY** are nonplanar with the dihedral angles of 39.84 (7)° between aromatic rings in **SECXAB** and 77.44(8)° in **TAMYOY**. Like in **DM4H**, the molecules of **TAMYOY** are interlinked by O-H···N and C-H···O bonding, whereas the molecules of **SECXAB** are interlinked by O-H···N and C-H···π interactions.

Powder XRD patterns (PXRD) of the simulation-based single-crystal XRD using a cif file were generated to get more details about the crystallinity of both compounds. This simulated XRD pattern represents sharp peaks for both **DC2H** and **DM4H** compounds (Figure S1). The results showed that the obtained compound is highly crystalline. Xpert HighScore Plus software was used to obtain the simulated pattern. The five most intense peaks were hkl-indexed on a simulation basis.

2.2. Hirshfeld Surface Analysis. The Hirshfeld surface (HS) analysis tool is used by crystallographers and crystal engineers to see strong and weak intermolecular interactions that also exert influence on the molecular packing in crystals. This analysis was performed using Crystal Explorer version 21.5.[28] HS was mapped over d_{norm} (function of normalized distances), d_e (distance from a specific point on the mapped surface to the closest atom outside), and d_i (distances from a particular point on the surface to the nearest atom inside).[29,30] HS d_{norm} mapping uses blue, white, and red colors to distinguish between the interatomic contacts that are longer, at Van der Waals separations, and short interatomic contacts, respectively.[31,32] Figure 5a,b represents the HS of **DC2H** and **DM4H** mapped with d_{norm} to view the distinctive red spots, demonstrating specific points of contact in the crystal (see close contacts in a unit cell Figure S2a,b). The red spots (bright and faint) can be classified as potential hydrogen bonds. The shape index property was used to map the HS views of **DC2H** and **DM4H**, which represent the red and blue triangular regions shown in Figure 5c,d, respectively. Here, bright-red spots indicate the $\pi\cdots\pi$ stacking between the six-membered rings.[33,34] Similarly, HS curvedness mapping also shows the $\pi\cdots\pi$ stacking, which is obvious because of the

https://doi.org/10.1021/acsomega.1c06325
ACS Omega 2022, 7, 5217−5230

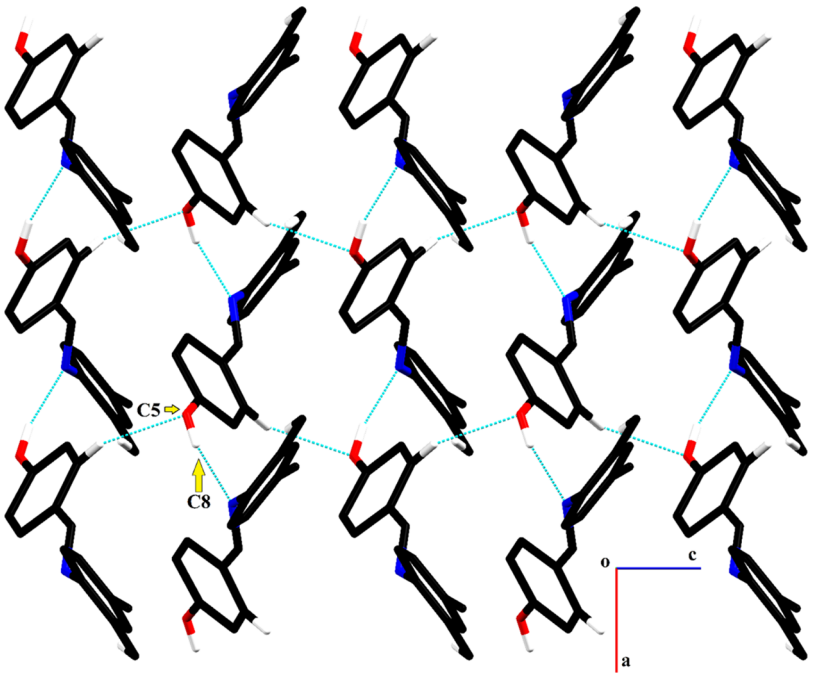

Figure 4. Packing diagram of **DM4H**: a view along the ac crystallographic plane. Only selected H-atoms are shown for clarity.

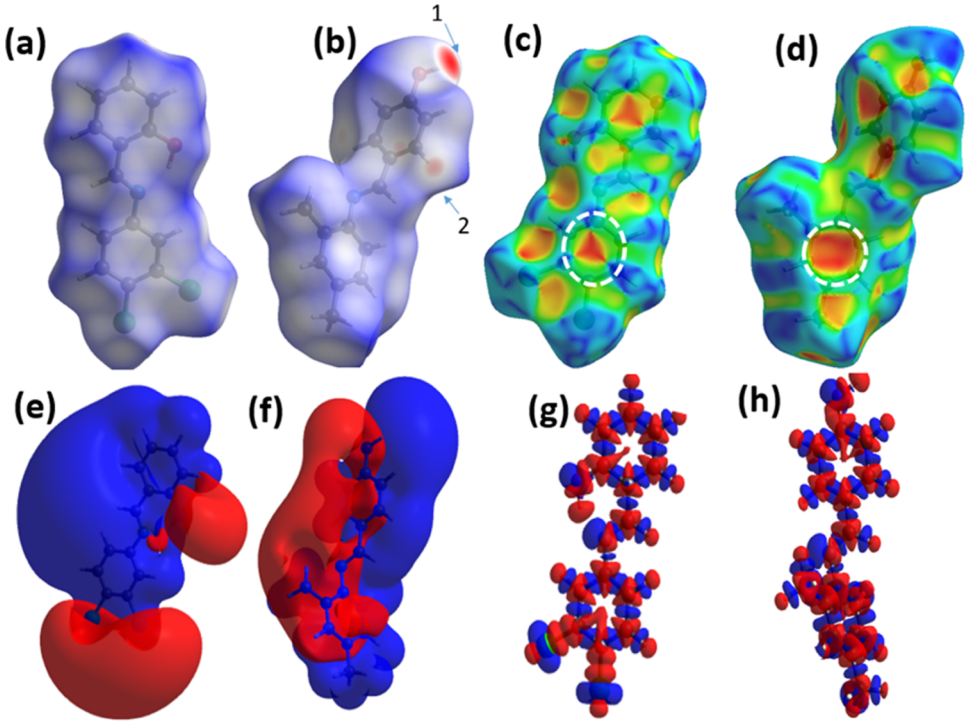

Figure 5. Hirshfeld surface (HS) of the **DC2H** mapped with d_{norm} (a). Hirshfeld surface (HS) of the **DM4H** mapped with d_{norm} (b), Hirshfeld surface of the **DC2H** and **DM4H** molecules drawn with shape index (c, d). Visualization of **DM4H** and **DC2H** molecules' electrostatic potential (e, f). The deformation density ($\pm$0.008 e au^{-3}) plot of **DM4H** and **DC2H** molecules (g, h).

flat regions around the carbon rings (Figure S3a,b). Figure 5e,f shows the electrostatic potential, while Figure 5g,h shows the deformation density for **DC2H** and **DM4H**, respectively. Deformation of the electron density is displayed with positive (blue) and negative (red) isosurfaces.

The 2D fingerprint plots are a way to explore the crystal packing of the single crystals in terms of interatomic contacts and their contribution to the crystal packing.[35,36] The important 2D fingerprint plots of **DC2H** are compared with the 2D fingerprint plots of a very closely related crystal structure obtained from the literature with the reference code **AWUSIV** and CCDC no. 841140. Similarly, important 2D fingerprint plots of **DM4H** are compared with the 2D fingerprint plots of a closely related crystal structure obtained from the literature with the reference code **TAMYOY** and CCDC no. 1491358. A comparative study of the important

https://doi.org/10.1021/acsomega.1c06325
ACS Omega 2022, 7, 5217−5230

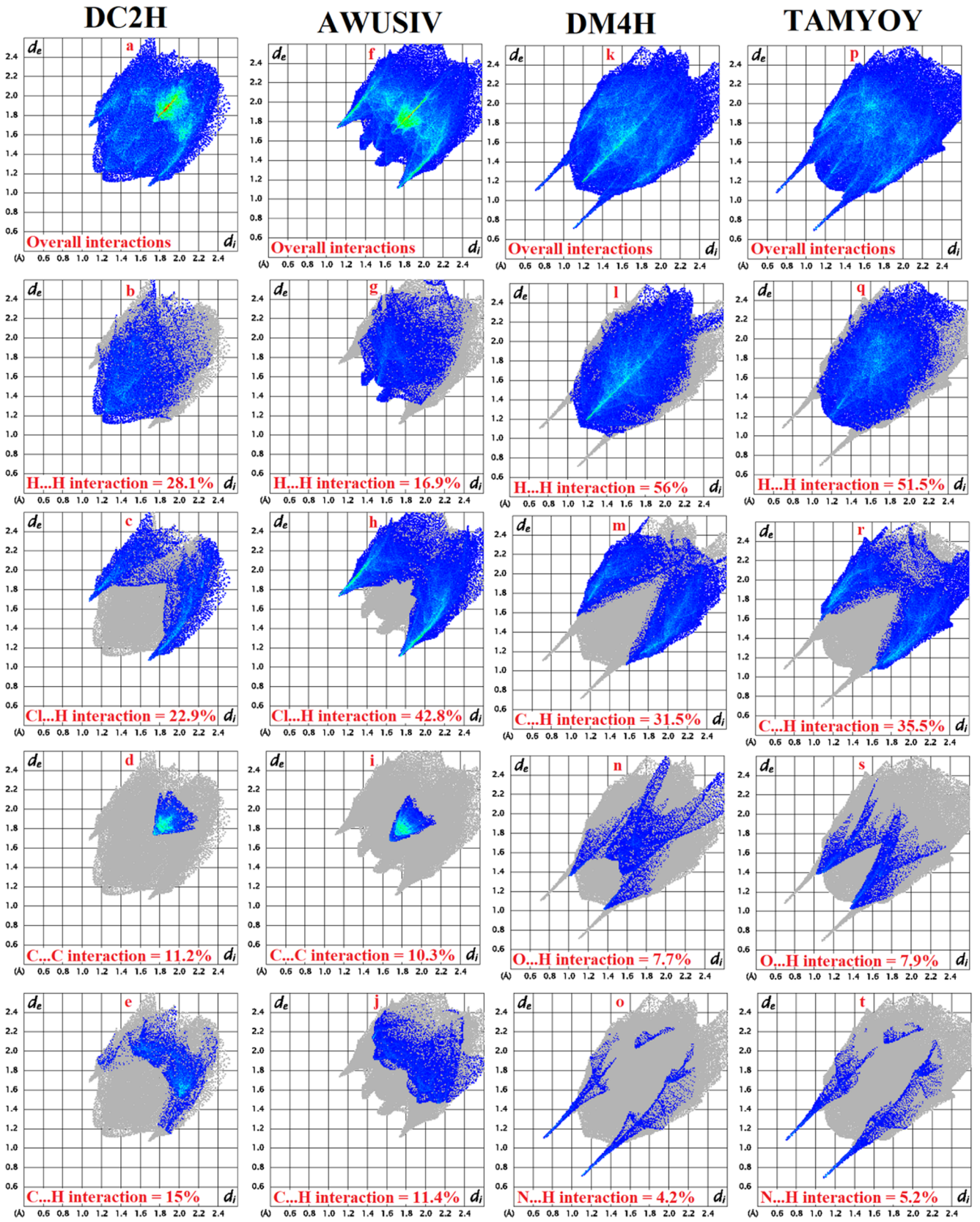

Figure 6. (a–e) Important 2D fingerprint plots of **DC2H**, (a) overall interactions and (b–e) individual interatomic contacts, which are compared with important 2D plots (f–j) of a crystal structure closely related to the **DC2H** found from the literature with the reference code **AWUSIV** and CCDC no. 841140. Similarly, Important 2D fingerprint plots (k–o) of **DM4H**, (k) overall interactions and (l–o) individual interatomic contacts, which are compared with important 2D plots (p–t) of a crystal structure closely related to **DM4H** found from the literature with the reference code **TAMYOY** and CCDC no. 1491358.

https://doi.org/10.1021/acsomega.1c06325
ACS Omega 2022, 7, 5217–5230

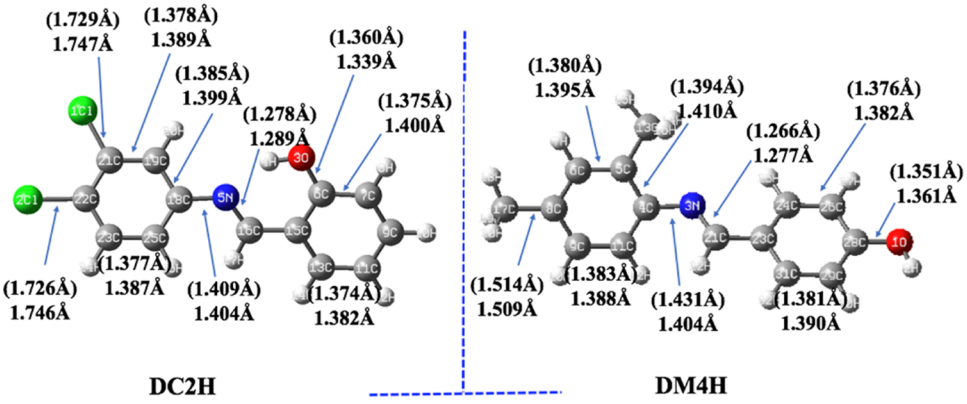

Figure 7. Optimized molecular geometries of compounds DC2H and DM4H where values in parenthesis are experimentally taken from crystal data.

2D fingerprint plots is shown in Figure 6. The central triangular region of sky-blue color in 2D fingerprint plots for overall interactions of **DC2H** (Figure 6a) and **AWUSIV** (Figure 6f) indicates the presence of the $\pi\cdots\pi$ stacking interaction in the crystal packing. The most important interatomic contact for **DC2H** is H···H with a percentage contribution of 28.1% (Figure 6b), whereas for **AWUSIV**, the most important interatomic contact is Cl···H with a percentage contribution of 42.8% (Figure 6h). In **AWUSIV**, the H···H interatomic contact has a percentage contribution of 16.9% (Figure 6g). The Cl···H interatomic contact has a larger contribution in **AWUSIV** as compared to in **DC2H** because the crystal structure of **AWUSIV** contains a trichloro-substituted phenyl ring, whereas the crystal structure of **DC2H** contains a dichloro-substituted phenyl ring. The 2D fingerprint plots for the overall interactions of **DM4H** and **TAMYOY** contain two large spikes. These spikes show an N···H contact with a percentage contribution of 4.2% in **DM4H** (Figures 6o) and 5.2% in **TAMYOY** (Figure 6t). The most important interatomic contact for **DM4H** and **TAMYOY** is H···H with a percentage contribution of 56% in **DM4H** (Figures 6l) and 51.5% in **TAMYOY** (Figure 6q). The 2D plots of C···H and O···H for **DM4H** and **TAMYOY** are also compared in Figure 6 with their contribution to the crystal packing.

Crystal Explorer 21.5 was used to calculate the interaction energy between pairs of molecules[37] (Figure S4a,b). The interaction energies were calculated based on two models: CE-B3LYP/6−31G(d,p) and CE-HF/3−21 G; furthermore, the 6−31 G basis set was used for both compounds. The total energy E was calculated in kJ/mol. E_{tot} is the individual sum of four factors: electrostatic (E_{ele}), polarization (E_{pol}), dispersion (E_{dis}), and exchange repulsion (E_{rep}). All calculations for the pairs of molecules are provided in Table S2 for **DM4H** and in Table S3 for **DC2H**. The total energy stabilizes the crystal packing with interaction energies of −32.8 kJ/mol (**DC2H**) and −57.6 kJ/mol (**DM4H**) for both molecules. Our analysis for these two molecules shows that they have the following components: electrostatic (4.5 kJ/mol), polarization (−3.2 kJ/mol), dispersion (−66.3 kJ/mol), and repulsion (+33.1 kJ/mol) for the **DC2H** molecule and electrostatic (−69.7 kJ/mol), polarization (−23.7 kJ/mol), dispersion (−34.6 kJ/mol), and repulsion (+74.0 kJ/mol) for the **DM4H** molecule. Based on the analysis of interactions in the crystal structure, it is implied that **DM4H** can be preferred at a supramolecular level.

The energy frameworks were simulated to give information about the contribution of the total energy.[38] Figure S5 shows the energy framework that gives visual understanding as cylinders joining the molecules (interaction pairs). Here, we fixed the radius of the cylinder at 100 kJ/mol. The color of the cylinders represents the specific type of energy, such as red cylinders for E_{ele} (Coulomb's interaction energy), green cylinders for E_{dis} (dispersion energy), and blue cylinders for E_{tot} (total energy). This approach is very useful for crystal engineers to deeply understand the mechanical behavior of the compounds at a molecular level. The energy frameworks revealed that the packing topology in terms of electrostatics is predominantly guided by **DM4H** and the dispersion energy topology is supported by $\pi\cdots\pi$ stacking.

3. COMPUTATIONAL RESULTS

3.1. Computational Methodology. All the quantum chemical calculations have been performed using the Gaussian 16 suite of programs.[39] The density functional theory method has been used to optimize the geometries of compounds **DC2H** and **DM4H** with the M06/6-31G* method. After optimizations, frequency calculations have been performed to get the global minimum structures with all positive frequencies for the compounds **DC2H** and **DM4H**. The AutoDock Vina program[40] is used for performing molecular docking studies with all default parameters. MGL tools[41] and Discovery Studio Visualizer[42] were used for input file preparation and output result visualization, respectively. Several attempts were made to get the most suitable docking models by doing several replicated docking calculations. Further essential details for protein and ligand preparations and other default parameters for docking studies can be seen in the Supporting Information of the article and also in our previous studies.[43]

3.2. Optimized Molecular Geometries of DC2H and DM4H. The optimized geometries of compounds **DC2H** and **DM4H** are given in Figure 7, where their respective experimental values are given in parenthesis. A careful analysis of Figure 7 shows that calculated and experimental geometries are in reasonable agreement. For **DC2H**, the experimental and calculated C_{18}-N_5 bonds are found to be 1.409 and 1.404 Å, respectively. Similarly, the experimental and calculated C_{16}-N_5 bonds are found to be 1.278 and 1.289 Å, respectively, in **DC2H**. The two calculated (experimental) halogen carbon bonds, C_{21}-Cl_1 and C_{22}-Cl_2, are illustrated as

https://doi.org/10.1021/acsomega.1c06325
ACS Omega 2022, 7, 5217−5230

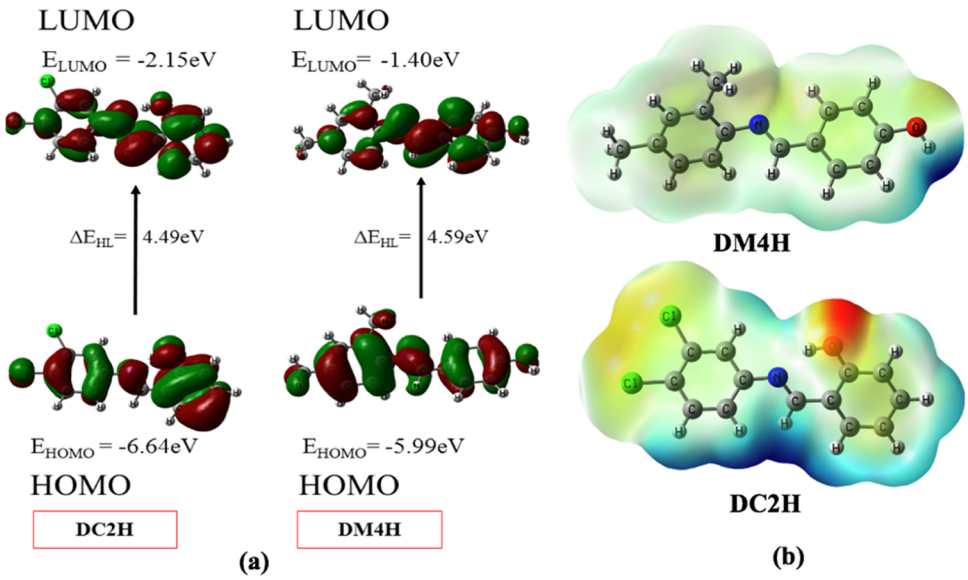

Figure 8. (a) HOMO and LUMO orbitals for compounds **DC2H** and **DM4H** and (b) molecular electrostatic potentials for compounds **DC2H** and **DM4H**, where positive and negative maxima are represented with blue and red color coding. The isovalues of 3D density surfaces are ±0.002 a. u.

1.729 Å (1.747 Å) and 1.726 (1.746) Å, respectively, in **DC2H**. For **DC2H**, the experimental and calculated C_6-O_{30} bonds are found to be 1.360 Å and 1.339 Å, respectively. A somewhat similar trend can also be seen among the calculated and experimental bond lengths of compound **DM4H** where only two heteroatoms, i.e., N and O, are involved in molecular geometry. For **DM4H**, its calculated (experimental) three crucial bonds, C_4-N_3, N_3-C_{21}, and C_{28}-O_1 are elucidated as 1.431 Å (1.404 Å), 1.277 Å (1.266 Å), and 1.361 Å (1.351) Å, respectively. Overall, most of the calculated bond distances are seen as larger than the experimental bond distances (values in parenthesis). This trend is justifiable because the current geometry optimizations were performed, in a vacuum while experimental crystal structures are in the solid state.

3.3. Frontier Molecular Orbitals (FMOs) and Molecular Electrostatic Potentials (MEPs). The FMOs play a very vital role in the reactivity and stability of molecular compounds. To comprehend the insights into the distribution of FMOs, we depict the HOMO and LUMO of the entitled compounds as shown in Figure 8a. There is a uniform distribution of electron density for the respective HOMO and LUMO orbitals over the surface of both entitled molecules. The dimethyl phenyl group of **DM4H** shows a slight donor behavior owing to its two methyl groups, where electron density moved away from the dimethyl phenyl moiety as seen in the HOMO and LUMO of **DM4H**. The HOMO−LUMO energy gaps of **DC2H** and **DM4H** compounds are also shown along with their individual orbital energies. The orbital energy gap of the **DM4H** compound is 4.59 eV, which is slightly larger (0.1 eV) as compared to that of **DC2H** (4.49 eV). The slight difference is due to the similar skeleton of both molecules. Furthermore, the electrostatic molecular potentials are also depicted to see the distributions of the local potential over the total electron density surface as color coding (Figure 8b). The red and blue colors indicate the negative and positive regions of electron density of the total electron density surface, respectively. In **DC2H** and **DM4H** molecules, the negative potentials are seen around the Cl and OH groups, making them vulnerable to electrophilic attacks, while positive regions can be seen as less prominent.

4. MOLECULAR DOCKING ANALYSIS

Computational chemistry has emerged significantly as a tool of trust with recent progress in algorithm developments. Molecular docking, a subfield of computational chemistry and bioscience, is providing several quick insights into the modern drug designing process. The cornerstone of molecular docking is based on the fact that most biological functions are controlled by specific proteins, and if a molecule shows the potential to interact with such specific proteins, it may also have the potential to inhibit the function of such proteins. Recently, several cutting-edge research reports from nature and science journals have also employed molecular docking methods to get insights into their research results.[44,45] Along these lines, two very crucial proteins, M^{pro} and NSP9 of SARS-CoV-2, are selected to study their interactions with indigenously synthesized ligands. Phenols constitute the largest class of bioactive compounds on the earth, which are usually formed through the secondary metabolites of plants. The antioxidant and anti-inflammatory properties of phenols are well-reported. Recent studies have highlighted their potential for possible antiviral potential as demonstrated by their efficacy against several pathogens, including influenza virus, enterovirus, and a class of coronaviruses.[46] As the COVID-19 disease (caused by SARS-CoV-2) has divested the world health sector and created a pandemic, it is very imperative to turn every stone to find a potential therapeutic drug candidate. Along the abovementioned lines, using molecular docking techniques, the current study also explores a few promising pieces of evidence for the antiviral potential of the above-entitled compounds.

4.1. Calculation of Binding Energy. The binding energy of docked ligands and protein molecules is a combination of many kinds of interaction energies, which are calculated during the docking of the ligand with a protein. Binding energy plays a crucial role in establishing the stability

https://doi.org/10.1021/acsomega.1c06325
ACS Omega 2022, 7, 5217−5230

Table 3. Binding Energy (Kcal/mol) and Inhibition Constant (Ki, μmol) of Docked Compounds DC2H and DM4H with M^{pro} and NSP9 Proteins

ligands	targeted protein	binding affinity	inhibition constant
DC2H	M^{pro}	−6.3	23.18
DM4H		−6.6	13.94
DC2H	NSP9	−6.5	16.52
DM4H		−6.5	16.52

of a ligand−protein complex. More negative binding energy reflects a more stable protein−ligand complex. Table 3 discloses the binding energy and inhibition constant values for both proteins (M^{pro} and NSP9). The binding energy values of **DC2H** and **DM4H** with M^{pro} are −6.3 and −6.6 kcal/mol, respectively (see Table 3). The inhibition constant values of these two compounds with M^{pro} and NSP9 are 23.18 and 13.94 μmol, respectively. **DC2H** and **DM4H** have similar binding energies and inhibition constant values with the NSP9 protein, which are −6.5 kcal/mol and 16.52 μmol, respectively (see Table 3). The negative binding energies indicate the favorable interactions of the synthesized compounds with M^{pro} and NSP9 proteins of SARS-CoV-2. Recently, Burkhanova et al. studied aniline dyes through molecular docking, which showed binding affinity towards M^{pro} with a binding energy value of about −7.6 kcal/mol.[47] A more relevant molecular docking study was about hydroxystilbamidine as M^{pro} inhibitors, where the imine group in the compound forms hydrogen bonds with aspartic acid moieties of M^{pro} as our current **DC2H** compound with histidine.[48] Furthermore, a semiquantitative comparison of binding energies of **DC2H** and **DM4H**, so-called standard drug molecules, shows that the binding energy with M^{pro} is better than the previously calculated value of chloroquine (−5.20 kcal/mol) and hydroxyl chloroquine (−5.60 kcal/mol) and comparable to that of Remdesivir (−7.00 kcal/mol),[49] which is a recently used drug against SARS-CoV-2.

4.2. Details of Intermolecular Interactions. The M^{pro} and NSP9 proteins show various intermolecular interactions, including H-bonds and hydrophobic and electrostatic interactions. All these interactions with amino acid residues and their bond lengths are given in Table 4 and Figure 9. Figure 9 shows 3D orientations, while an overview of 2D interactions is provided in Figure S6 of the Supporting Information for ligand−protein interactions where both types of visualizations are commonly used in molecular docking studies. **DC2H** exhibited two conventional H-bond interactions with His41 (2.41 Å) and Gln189 (2.22 Å) amino acid residues of M^{pro}. It also shows two electrostatic interactions with His41 (2.90 Å) and Cys145 (4.99 Å) amino acid residues. **DC2H** exhibits three hydrophobic interactions, which are alkyl, π-alkyl, and π···π stacking interactions with Met49 (5.12 Å), Met165 (4.82 Å), and His41 (4.83 Å) amino acid residues, respectively. In interactions of **DC2H** with M^{pro}, the amino acid residue His41 has an active role as it revealed all H-bonds and hydrophobic and electrostatic interactions. **DC2H** with NSP9 showed two types of interactions: conventional H-bonding and hydrophobic interactions. The conventional H-bonding interactions are with Gly38 (2.36 Å) and Gly39 (2.54 Å) amino acid residues. The hydrophobic interactions are with Phe41 (4.06 Å), Phe57 (4.20 Å, 5.18 Å), Ile92 (4.34 Å), Ile66 (4.21 Å), and Val42 (3.90 Å, 3.70 Å, and 5.43 Å). Figure 9 shows the

Table 4. All Interactions, along with Associated Residues and Respective Bond Lengths, between Receptor M^{pro} and Spike Proteins of SARS-CoV-2 and Compounds DC2H and DM4H with the Highest Binding Energies

	interactions with associated residues and bond length		
ligands	hydrogen bond	hydrophobic interactions	electrostatic and others
DC2H-M^{pro}	(1) His41 (2.41)	(1) Met49 (5.12)	(1) Cys145 (4.99)
	(2) Gln189 (2.22)	(2) Met165 (4.82)	(2) His41 (2.90)
		(3) His41 (4.83)	
DC2H-NSP9	(1) Gly38 (2.36)	(1) Phe41 (4.06)	
	(2) Gly39 (2.54)	(2) Ile92 (4.34)	
		(3) Phe57 (4.20)	
		(4) Phe57 (5.18)	
		(5) Ile66 (4.21)	
		(6) Val42 (3.90)	
		(7) Val42 (3.70)	
		(8) Val42 (5.43)	
DM4H-M^{pro}	(1) Phe140 (2.53)	(1) His41 (3.97)	(1) Cys145 (5.60)
		(2) His41 (4.35)	(2) Met165 (5.68)
		(3) Met49 (3.96)	
		(4) Met49 (4.71)	
DM4H-NSP9	(1) Pro58 (2.72)	(1) Phe41 (4.98)	
	(2) Arg40 (2.66)	(2) Phe41 (5.29)	
		(3) Val42 (5.20)	
		(4) Ile92 (4.87)	
		(5) Ile92 (5.33)	
		(6) Phe57 (4.31)	
		(7) Ile66 (5.25)	

3D interactions of **DC2H** with M^{pro} and NSP9 proteins. **DM4H** also revealed various interactions with M^{pro} and NSP proteins. With M^{pro}, it showed one conventional H-bond and two electrostatic and four hydrophobic interactions. The conventional H-bond interactions are with Phe140 (2.53 Å), electrostatic interactions are with Cys145 (5.60 Å) and Met165 (5.68 Å), hydrophobic interactions are with His41 (3.97 Å and 4.35 Å) and Met49 (3.96 Å and 4.71 Å). It showed seven hydrophobic and two conventional H-bond interactions with the NSP9 protein. The conventional H-bond interactions are with Pro58 (2.72 Å) and Arg40 (2.66 Å) amino acid residues. The hydrophobic interactions are with Phe41 (4.98 Å, and 5.29 Å), Val42 (5.20 Å), Ile92 (4.87 Å, and 5.33 Å), Phe57 (4.31 Å), and Ile66 (5.25 Å) amino acid residues.

Interestingly, as all the interactions between ligands and proteins can be broadly divided as polar and nonpolar, we have presented the density surface representations of polar and nonpolar interacting residues of the binding pockets as shown in Figure S7. The interactions of **DC2H** and **DM4H** with the M^{pro} protein are represented in Figure S7a,b, respectively, where the total density surface of the protein is illustrated in cyan, polar areas are symbolized in magenta, and nonpolar areas are illustrated in yellow. The Nsp9 interactions with **DC2H** and **DM4H** are illustrated in Figure S7c,d, where the total density surface of the protein is shown in a warm-pink color, the polar area is denoted in green, and the nonpolar area are shown in yellow. An overview of polar and nonpolar surfaces signifies their respective contributions

https://doi.org/10.1021/acsomega.1c06325
ACS Omega 2022, 7, 5217−5230

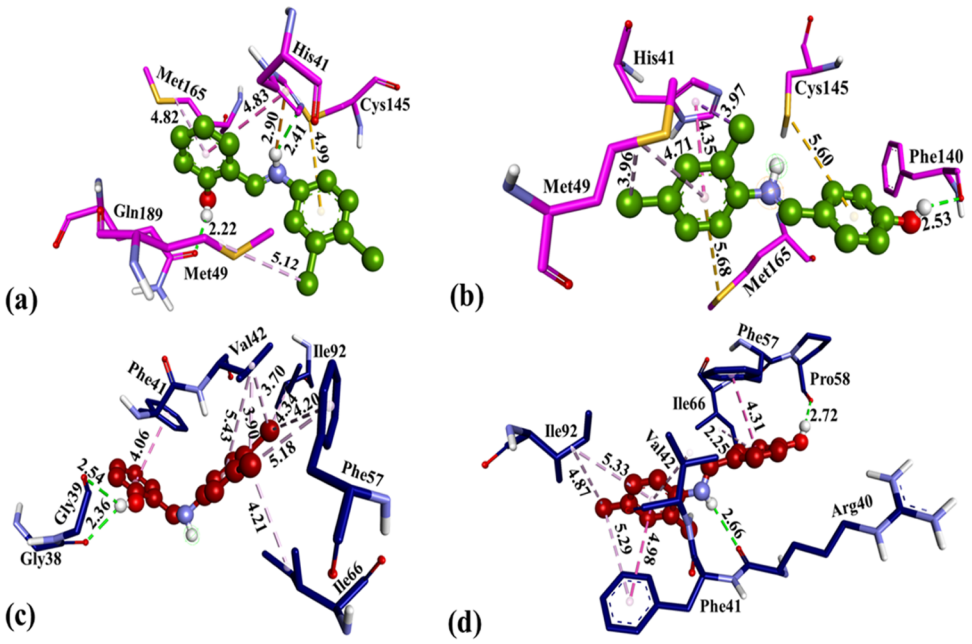

Figure 9. 3D interactions of **DC2H** and **DM4H** with amino acid residues of M^{pro} (pink) and Nsp9 (blue) proteins; (a and b) 3D interactions of **DC2H** and **DM4H** with the M^{pro} protein, respectively; and (c and d) 3D interactions of **DC2H** and **DM4H** with the Nsp9 protein, respectively.

Scheme 1. Synthesis of Schiff bases DC2H and DM4H

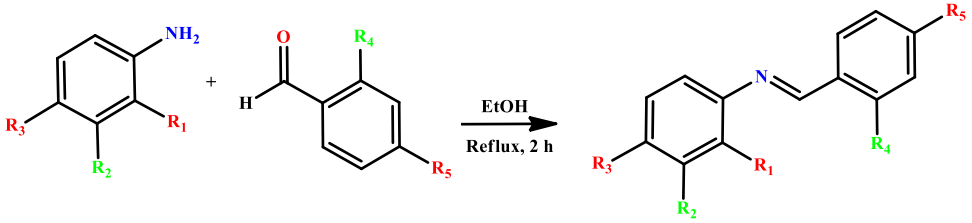

DC2H: R_2 & R_3 = Cl , R_1 & R_5 = H, R_4 = OH

DM4H: R_1 & R_3 = CH_3 , R_2 & R_4 = H, R_5 = OH

to assessing the nature of interactions in a semiquantitative way.

5. CONCULSIONS AND PERSPECTIVES

Two crystalline imine compounds, **DC2H** and **DM4H**, are synthesized efficiently, and their crystal structures are confirmed using the single-crystal X-ray diffraction technique. The crystal structures of these compounds are fully explored in terms of molecular configuration, intramolecular H-bonding, and intermolecular H-bonding. Moreover, a Cambridge Structural Database (CSD) search is carried out to find closely related crystal structures, and then, these crystal structures are compared with those of **DC2H** and **DM4H**. Intermolecular interactions that are the main aspect of the crystal packing of both compounds are further explored by Hirshfeld surface analysis. The quantum chemical and molecular docking calculations were performed to study the optoelectronic and antiviral potential of the synthesized compounds. The possible inhibition properties against two very crucial proteins (M^{pro} and NSP9) of SARS-CoV-2 were studied through molecular docking. The calculated binding energies of **DC2H** and **DM4H** with M^{pro} are found to be -6.3 and -6.6 kcal/mol, respectively, where negative energies indicate the favorable interactions of the synthesized compounds with the above-studied proteins of SARS-CoV-2. Thus, we have successfully not only synthesized these compounds but also investigated their potential functional properties.

6. EXPERIMENTAL SECTION

6.1. Material and Methods. The different solvents and precursors employed in the present experimental work were highly pure and purchased from Acros Organics, Alfa Aesar, and Sigma-Aldrich/Merck and were used as received.

6.2. Synthesis of Schiff Bases DC2H and DM4H. The precursors, 2,4-dimethylaniline or 3,4-dichloroaniline (5 mmol), were dissolved in 25 mL of ethanol, to which an ethanolic solution (25 mL) of equimolar quantities (5 mmol) of 2-hydroxybenzaldehyde or 4-hydroxybenzaldehyde was added dropwise. The reactants were refluxed for 2 h, and then, the clear solution was left for crystallization until the light-yellow needle-shaped crystals of **DC2H** and colorless rod-like crystals of **DM4H** were grown at the bottom and along the sidewall of the container. The crystals were separated by decantation and then dried gently under the folds of filter paper (Scheme 1).

https://doi.org/10.1021/acsomega.1c06325
ACS Omega 2022, 7, 5217−5230

6.3. X-ray Data Collection and Refinement Details.

We collected the X-ray data of **DC2H** and **DM4H** on a Bruker Kappa Apex-II CCD diffractometer. The diffractometer contains an X-ray tube to generate monochromatic rays (λ = 0.71073 Å). Bruker APEX-II,[50] SHELXS-97,[51] and SHELXL 2018/3[52] are employed for data collection, structure solution, and refinement, respectively. Refinement of all nonhydrogen atoms is performed using ADP (anisotropic displacement parameters), while the refinement of H-atoms is performed using isotropic displacement parameters and using the riding model. The H-atoms are inspected by the keen observation of residual peaks using refinement of data. Mercury 4.0[53] and Platon[54] software tools are employed for the sake of graphics related to XRD.

■ ASSOCIATED CONTENT

Supporting Information

The Supporting Information is available free of charge at https://pubs.acs.org/doi/10.1021/acsomega.1c06325.

PXRD stick-like patterns of the simulation by single-crystal analysis of **DC2H** and **DM4H** using Xpert High Score Plus software (Figure S1); HS over d_{norm} with the neighboring molecules for **DC2H** and **DM4H** (Figure S2); HS plotted over curvedness in the range from −0.4 to 4 a.u. for **DC2H** and **DM4H** (Figure S3); interaction energies based on unperturbed electron distributions computed at the B3LYP level of theory employing the 6−31G basis set and scaled appropriately for **DC2H** and **DM4H** (Figure S4); energy frameworks of E_{ele} (coulomb energy), E_{dis} (dispersion energy), and E_{tot} total energy diagrams of **DC2H** and **DM4H** (Figure S5); 2D interactions of **DC2H** and **DM4H** with amino acid residues of M^{pro} (green ligands) and Nsp9 (red ligands) proteins, 2D interactions of **DC2H** and **DM4H** with the M^{pro} protein, 2D interactions of **DC2H** and **DM4H** with the Nsp9 protein (Figure S6); density surface representation of polar and nonpolar interactions of M^{pro} and Nsp9 proteins in their binding pockets, and interactions of **DC2H** and **DM4H** with the M^{pro} protein (Figure S7); hydrogen-bond geometry (Å, deg) for **DC2H** and **DM4H** (Table S1); interaction energies of **DC2H** using Crystal Explorer 21 (in kJ/mol) (Table S2); interaction energies of **DM4H** using Crystal Explorer 21 (in kJ/mol) (Table S3) (PDF)

Crystallographic data of DM4H (CIF)

Crystallographic data of DC2H (CIF)

■ AUTHOR INFORMATION

Corresponding Authors

Muhammad Ashfaq − *Department of Physics, University of Sargodha, Sargodha 40100, Pakistan;* Present Address: Department of Physics, University of Mianwali, Mianwali 42200, Pakistan; orcid.org/0000-0001-6663-8777; Email: muhammadashfaq1400@gmail.com

Khurram Shahzad Munawar − *Institute of Chemistry, University of Sargodha, Sargodha 40100, Pakistan;* Present Address: Department of Chemistry, University of Mianwali, Mianwali 42200, Pakistan; orcid.org/0000-0001-9055-2519; Email: khurramchemist@gmail.com

Authors

Muhammad Nawaz Tahir − *Department of Physics, University of Sargodha, Sargodha 40100, Pakistan*

Shabbir Muhammad − *Department of Chemistry, College of Science, King Khalid University, Abha 61413, Saudi Arabia;* orcid.org/0000-0003-4908-3313

Saqib Ali − *Department of Chemistry, Quaid-i-Azam University, Islamabad 45320, Pakistan*

Gulzar Ahmed − *School of Materials Science and Engineering, South China University of Technology, Guangzhou 510640, China;* Present Address: Department of Physics, University of Mianwali, Mianwali 42200, Pakistan

Abdullah G. Al-Sehemi − *Department of Chemistry, College of Science, King Khalid University, Abha 61413, Saudi Arabia;* orcid.org/0000-0002-6793-3038

Saleh S. Alarfaji − *Department of Chemistry, College of Science, King Khalid University, Abha 61413, Saudi Arabia;* orcid.org/0000-0001-7297-7185

Muhammad Ehtisham Ibraheem Khan − *Department of Chemistry, University of Wah, Rawalpindi 47040, Pakistan;* orcid.org/0000-0003-4420-8404

Complete contact information is available at: https://pubs.acs.org/10.1021/acsomega.1c06325

Notes

The authors declare no competing financial interest.

■ ACKNOWLEDGMENTS

The authors extend their appreciation to the Deanship of Scientific Research at King Khalid University for funding the work through the Research Project (RGP.2/156/42). For computer time, this research used the resources of the Supercomputing Laboratory at King Abdullah University of Science & Technology (KAUST) in Thuwal, Saudi Arabia.

■ REFERENCES

(1) Schiff, H. Mittheilungen aus dem Universitätslaboratorium in Pisa: eine neue Reihe organischer Basen. *Ann. Chem.* **1864**, *131*, 118−119.

(2) Munawar, K. S.; Haroon, S. M.; Hussain, S. A.; Raza, H. Schiff bases: multipurpose pharmacophores with extensive biological applications. *J. Basic Appl. Sci.* **2018**, *14*, 217−229.

(3) Iacopetta, D.; Ceramella, J.; Catalano, A.; Saturnino, C.; Bonomo, M. G.; Franchini, C.; Sinicropi, M. S. Schiff Bases: Interesting Scaffolds with Promising Antitumoral Properties. *Appl. Sci.* **2021**, *11*, No. 1877.

(4) (a) Rauf, A.; Shah, A.; Munawar, K. S.; Ali, S.; Tahir, M. N.; Javed, M.; Khan, A. M. Synthesis, physicochemical elucidation, biological screening and molecular docking studies of a Schiff base and its metal (II) complexes. *Arab. J. Chem.* **2020**, *13*, 1130−1141. (b) Munawar, K. S.; Ali, S.; Tahir, M. N.; Khalid, N.; Abbas, Q.; Qureshi, I. Z.; Hussain, S.; Ashfaq, M. Synthesis, spectroscopic characterization, X-ray crystal structure, antimicrobial, DNA-binding, alkaline phosphatase and insulin-mimetic studies of oxidovanadium (IV) complexes of azomethine precursors. *J Coord Chem.* **2020**, *73*, 2275−2300. (c) Abbas, S.; Zaib, S.; Ur Rahman, S.; Ali, S.; Hameed, S.; Tahir, M. N.; Munawar, K. S.; Shaheen, F.; Abbas, S. M.; Iqbal, J. Carbonic Anhydrase Inhibitory Potential of 1, 2, 4-triazole-3-thione Derivatives of Flurbiprofen, Ibuprofen and 4-tert-butylbenzoic Hydrazide: Design, Synthesis, Characterization, Biochemical Evaluation, Molecular Docking and Dynamic Simulation Studies. *Med. Chem.* **2019**, *15*, 298−310. (d) Rauf, A.; Shah, A.; Munawar, K. S.; Khan, A. A.; Abbasi, R.; Yameen, M. A.; Khan, A. M.; Khan, A. R.; Qureshi, I. Z.; Kraatz, H. B. Synthesis, spectroscopic character-

https://doi.org/10.1021/acsomega.1c06325
ACS Omega 2022, 7, 5217−5230

ization, DFT optimization and biological activities of Schiff bases and their metal (II) complexes. *J. Mol. Struct.* **2017**, *1145*, 132−140.
(5) (a) Shabbir, M.; Akhter, Z.; Ahmad, I.; Ahmed, S.; Shafiq, M.; Mirza, B.; McKee, V.; Munawar, K. S.; Ashraf, A. R. Schiff base triphenylphosphine palladium (II) complexes: Synthesis, structural elucidation, electrochemical and biological evaluation. *J. Mol. Struct.* **2016**, *1118*, 250−258. (b) Konda, R. K.; Kumar, A.; Asif, M.; Reddy, A. Synthesis, characterization and anti-bacterial activity of novel schiff bases of pyridin-3 yl-carbohydrazide derivatives. *J. Innovations Appl. Pharm. Sci.* **2021**, 23−26. (c) Salvat, A.; Antonnacci, L.; Fortunato, R. H.; Suárez, E. Y.; Godoy, H. M. Screening of some plants from Northern Argentina for their antimicrobial activity. *Lett. Appl. Microbiol.* **2001**, *32*, 293−297.
(6) (a) Uddin, M. N.; Ahmed, S. S.; Alam, S. R. Biomedical applications of Schiff base metal complexes. *J. Coord. Chem.* **2020**, *73*, 3109−3149. (b) Jeevadason, A. W.; Murugavel, K. K.; Neelakantan, M. A. Review on Schiff bases and their metal complexes as organic photovoltaic materials. *Renewable Sustainable Energy Rev.* **2014**, *36*, 220−227. (c) More, M. S.; Joshi, P. G.; Mishra, Y. K.; Khanna, P. K. Metal complexes driven from Schiff bases and semicarbazones for biomedical and allied applications: a review. *Mater. Today Chem.* **2019**, *14*, No. 100195.
(7) (a) Irfan, R. M.; Shaheen, M. A.; Saleem, M.; Tahir, M. N.; Munawar, K. S.; Ahmad, S.; Rubab, S. L.; Tahir, T.; Kotwica-Mojzych, K.; Mojzych, M. Synthesis of new cadmium (II) complexes of Schiff bases as alkaline phosphatase inhibitors and their antimicrobial activity. *Arab. J. Chem.* **2021**, *14*, No. 103308. (b) Irfan, R. M.; Khan, S. A.; Tahir, M. H.; Ahmad, T.; Ali, L.; Afzal, M.; Ali, H.; Abbas, A.; Munawar, K. S.; Zhao, J.; Gao, L. Integration of an aminopyridine derived cobalt based homogenous cocatalyst with a composite photocatalyst to promote H 2 evolution from water. *New J. Chem.* **2021**, *45*, 5561−5567.
(8) Kaya, S.; Erkan, S.; Karakaş, D. Computational investigation of molecular structures, spectroscopic properties and antitumor-antibacterial activities of some Schiff bases. *Spectrochim. Acta, Part A* **2021**, *244*, No. 118829.
(9) Sumrra, S. H.; Zafar, W.; Asghar, M. L.; Mushtaq, F.; Raza, M. A.; Nazar, M. F.; Nadeem, M. A.; Imran, M.; Mumtaz, S. Computational investigation of molecular structures, spectroscopic properties, cholinesterase inhibition and antibacterial activities of triazole Schiff bases endowed metal chelates. *J. Mol. Struct.* **2021**, *1238*, No. 130382.
(10) Zafar, W.; Sumrra, S. H.; Chohan, Z. H. A Review: Pharmacological Aspects of Metal Based 1, 2, 4-Triazole Derived Schiff Bases. *Eur. J. Med. Chem.* **2021**, *222*, No. 113602.
(11) (a) Iacopetta, D.; Ceramella, J.; Catalano, A.; Saturnino, C.; Bonomo, M. G.; Franchini, C.; Sinicropi, M. S. Schiff Bases: Interesting Scaffolds with Promising Antitumoral Properties. *Appl. Sci.* **2021**, *11*, No. 1877. (b) Munawar, K. S.; Ali, S.; Tahir, M. N.; Khalid, N.; Abbas, Q.; Qureshi, I. Z.; Shahzadi, S. Investigation of derivatized schiff base ligands of 1, 2, 4-triazole amine and their oxovanadium (IV) complexes: Synthesis, structure, DNA binding, alkaline phosphatase inhibition, biological screening, and insulin mimetic properties. *Russ. J. Gen. Chem.* **2015**, *85*, 2183−2197.
(12) Verma, C.; Quraishi, M. A. Recent progresses in Schiff bases as aqueous phase corrosion inhibitors: Design and applications. *Coord. Chem. Rev.* **2021**, *446*, No. 214105.
(13) Abd-Elzaher, M. M.; Labib, A. A.; Mousa, H. A.; Moustafa, S. A.; Ali, M. M.; El-Rashedy, A. A. Synthesis, anticancer activity and molecular docking study of Schiff base complexes containing thiazole moiety. *Beni-Seuf Univ. J. Basic Appl. Sci.* **2016**, *5*, 85−96.
(14) Howsaui, H. B.; Basaleh, A. S.; Abdellattif, M. H.; Hassan, W. M.; Hussien, M. A. Synthesis, Structural Investigations, Molecular Docking, and Anticancer Activity of Some Novel Schiff Bases and Their Uranyl Complexes. *Biomolecules* **2021**, *11*, No. 1138.
(15) Ghanghas, P.; Choudhary, A.; Kumar, D.; Poonia, K. Coordination Metal Complexes with Schiff bases: Useful Pharmacophores with Comprehensive Biological Applications. *Inorg. Chem. Commun.* **2021**, *130*, No. 108710.
(16) Chaturvedi, D.; Kamboj, M. Role of Schiff base in drug discovery research. *Chem. Sci. J.* **2016**, *7*, No. e114.
(17) Kajal, A.; Bala, S.; Kamboj, S.; Sharma, N.; Saini, V. Schiff bases: a versatile pharmacophore. *J. Catal.* **2013**, *2013*, 1−14.
(18) Jarrahpour, A.; Khalili, D.; De Clercq, E.; Salmi, C.; Brunel, J. M. Synthesis, antibacterial, antifungal and antiviral activity evaluation of some new bis-Schiff bases of isatin and their derivatives. *Molecules* **2007**, *12*, 1720−1730.
(19) Bhattacharya, A.; Purohit, V. C.; Rinaldi, F. Environmentally friendly solvent-free processes: novel dual catalyst system in Henry reaction. *Org. Process Res. Dev.* **2003**, *7*, 254−258.
(20) (a) Martin, A. D.; Hartlieb, K. J.; Sobolev, A. N.; Raston, C. L. Hirshfeld surface analysis of substituted phenols. *Cryst. Growth Des.* **2010**, *10*, 5302−5306. (b) Ahmed, M. N.; Ghias, M.; Shah, S. A.; Shoaib, M.; Tahir, M. N.; Ashfaq, M.; Ibrahim, M. A.; Andleeb, H.; Gil, D. M.; Frontera, A. X-Ray characterization, Hirshfeld surface analysis, DFT calculations, in vitro and in silico lipoxygenase inhibition (LOX) studies of dichlorophenyl substituted 3-hydroxy-chromenones. *New J. Chem.* **2021**, *45*, 19928−19940. (c) Kargar, H.; Fallah-Mehrjardi, M.; Behjatmanesh-Ardakani, R.; Munawar, K. S.; Ashfaq, M.; Tahir, M. N. Diverse coordination of isoniazid hydrazone Schiff base ligand towards iron (III): Synthesis, characterization, SC-XRD, HSA, QTAIM, MEP, NCI, NBO and DFT study. *J. Mol. Struct.* **2021**, *1250*, No. 131691.
(21) (a) Kargar, H.; Behjatmanesh-Ardakani, R.; Torabi, V.; Kashani, M.; Chavoshpour-Natanzi, Z.; Kazemi, Z.; Mirkhani, V.; Sahraei, A.; Tahir, M. N.; Ashfaq, M.; Munawar, K. S. Synthesis, characterization, crystal structures, DFT, TD-DFT, molecular docking; DNA binding studies of novel copper (II); zinc (II) complexes bearing halogenated bidentate N, O-donor Schiff base ligands. *Polyhedron* **2021**, *195*, No. 114988. (b) Kargar, H.; Aghaei-Meybodi, F.; Elahifard, M. R.; Tahir, M. N.; Ashfaq, M.; Munawar, K. S. Some new Cu (II) complexes containing O, N-donor Schiff base ligands derived from 4-aminoantipyrine: synthesis, characterization, crystal structure and substitution effect on antimicrobial activity. *J. Coord. Chem.* **2021**, 1−13.
(22) (a) Kargar, H.; Behjatmanesh-Ardakani, R.; Torabi, V.; Sarvian, A.; Kazemi, Z.; Chavoshpour-Natanzi, Z.; Mirkhani, V.; Sahraei, A.; Tahir, M. N.; Ashfaq, M. Novel copper (II) and zinc (II) complexes of halogenated bidentate N, O-donor Schiff base ligands: Synthesis, characterization, crystal structures, DNA binding, molecular docking, DFT and TD-DFT computational studies. *Inorganica Chim. Acta.* **2021**, *514*, No. 120004. (b) Kargar, H.; Aghaei-Meybodi, F.; Behjatmanesh-Ardakani, R.; Elahifard, M. R.; Torabi, V.; Fallah-Mehrjardi, M.; Tahir, M. N.; Ashfaq, M.; Munawar, K. S. Synthesis, crystal structure, theoretical calculation, spectroscopic and antibacterial activity studies of copper (II) complexes bearing bidentate Schiff base ligands derived from 4-aminoantipyrine: influence of substitutions on antibacterial activity. *J. Mol. Struct.* **2021**, *1230*, No. 129908. (c) Kargar, H.; Ardakani, A. A.; Tahir, M. N.; Ashfaq, M.; Munawar, K. S. Synthesis, spectral characterization, crystal structure; antibacterial activity of nickel (II), copper (II) and zinc (II) complexes containing ONNO donor Schiff base ligands. *J. Mol. Struct.* **2021**, *1233*, No. 130112.
(23) (a) Kargar, H.; Ardakani, A. A.; Tahir, M. N.; Ashfaq, M.; Munawar, K. S. Synthesis, spectral characterization, crystal structure determination and antimicrobial activity of Ni (II), Cu (II) and Zn (II) complexes with the Schiff base ligand derived from 3, 5-dibromosalicylaldehyde. *J. Mol. Struct.* **2021**, *1229*, No. 129842. (b) Kargar, H.; Ardakani, A. A.; Munawar, K. S.; Ashfaq, M.; Tahir, M. N. Nickel (II), copper (II) and zinc (II) complexes containing symmetrical Tetradentate Schiff base ligand derived from 3, 5-diiodosalicylaldehyde: Synthesis, characterization, crystal structure and antimicrobial activity. *J. Iran. Chem. Soc.* **2021**, 1−11.
(24) Fun, H. K.; Quah, C. K.; Viveka, S.; Madhukumar, D. J.; Nagaraja, G. K. 2-[(E)-(2, 4, 6-Trichlorophenyl) iminomethyl] phenol. *Acta Crystallogr., Sect. E: Struct. Rep. Online* **2011**, *67*, o1934.
(25) Allaway, C. L.; Daly, M.; Nieuwenhuyzen, M.; Saunders, G. C. Synthesis of polyfluorodibenz [b, f][1, 4] oxazepines by the

https://doi.org/10.1021/acsomega.1c06325
ACS Omega 2022, 7, 5217−5230

cyclization of 2-[(polyfluorobenzylidene) amino] phenols. *J. Fluor. Chem.* **2002**, *115*, 91−99.
(26) Manjunath, B. C.; Abdoh, M. M. M.; Mallesha, L.; Mohana, K. N.; Lokanath, N. K. 4-[(3-Chloro-2-methylphenyl) iminomethyl] phenol. *Acta Crystallogr., Sect. E: Struct. Rep. Online* **2012**, *68*, o3191.
(27) Elemike, E. E.; Nwankwo, H. U.; Onwudiwe, D. C.; Hosten, E. C. Synthesis, structures, spectral properties and DFT quantum chemical calculations of (E)-4-(((4-propylphenyl) imino) methyl) phenol and (E)-4-((2-tolylimino) methyl) phenol; their corrosion inhibition studies of mild steel in aqueous HCl. *J. Mol. Struct.* **2017**, *1141*, 12−22.
(28) (a) Spackman, P. R.; Turner, M. J.; McKinnon, J. J.; Wolff, S. K.; Grimwood, D. J.; Jayatilaka, D.; Spackman, M. A. CrystalExplorer: a program for Hirshfeld surface analysis, visualization and quantitative analysis of molecular crystals. *J. Appl. Crystallogr.* **2021**, *54*, 1006−1011. (b) Kargar, H.; Fallah-Mehrjardi, M.; Behjatmanesh-Ardakani, R.; Torabi, V.; Munawar, K. S.; Ashfaq, M.; Tahir, M. N. Sonication-assisted synthesis of new Schiff bases derived from 3-ethoxysalicylaldehyde: Crystal structure determination, Hirshfeld surface analysis, theoretical calculations and spectroscopic studies. *J. Mol. Struct.* **2021**, *1243*, No. 130782.
(29) (a) Spackman, M. A.; Jayatilaka, D. Hirshfeld surface analysis. *CrystEngComm* **2009**, *11*, 19−32. (b) Tahir, M. N.; Ashfaq, M.; Alexander, F. D. L. T.; Caballero, J.; Hernández-Rodríguez, E. W.; Ali, A. Rationalizing the stability and interactions of 2, 4-diamino-5-(4-chlorophenyl)-6-ethylpyrimidin-1-ium 2-hydroxy-3, 5-dinitrobenzoate salt. *J. Mol. Struct.* **2019**, *1193*, 185−194. (c) Ashfaq, M.; Tahir, M. N.; Kuznetsov, A.; Mirza, S. H.; Khalid, M.; Ali, A. DFT and single crystal analysis of the pyrimethamine-based novel co-crystal salt: 2, 4-diamino-5-(4-chloro-phenyl)-6-ethylpyrimidin-1-ium: 4-hydroxybenzoate: methanol: hydrate (1: 1: 1: 1)(DEHMH). *J. Mol. Struct.* **2020**, *1199*, No. 127041.
(30) (a) Ali, A.; Khalid, M.; Rehman, M. F. U.; Haq, S.; Ali, A.; Tahir, M. N.; Ashfaq, M.; Rasool, F.; Braga, A. A. C. Efficient synthesis, SC-XRD, and theoretical studies of O-benzenesulfonylated pyrimidines: role of noncovalent interaction influence in their supramolecular network. *ACS omega* **2020**, *5*, 15115−15128. (b) Ali, A.; Khalid, M.; Tahir, M. N.; Imran, M.; Ashfaq, M.; Hussain, R.; Assiri, M. A.; Khan, I. Synthesis of Diaminopyrimidine Sulfonate Derivatives and Exploration of Their Structural and Quantum Chemical Insights via SC-XRD and the DFT Approach. *ACS omega* **2021**, *6*, 7047−7057.
(31) (a) Kargar, H.; Forootan, P.; Fallah-Mehrjardi, M.; Behjatmanesh-Ardakani, R.; Rudbari, H. A.; Munawar, K. S.; Ashfaq, M.; Tahir, M. N. Novel oxovanadium and dioxomolybdenum complexes of tridentate ONO-donor Schiff base ligand: Synthesis, characterization, crystal structures, Hirshfeld surface analysis, DFT computational studies and catalytic activity for the selective oxidation of benzylic alcohols. *Inorganica Chim. Acta.* **2021**, *523*, No. 120414. (b) Kargar, H.; Fallah-Mehrjardi, M.; Behjatmanesh-Ardakani, R.; Munawar, K. S.; Ashfaq, M.; Tahir, M. N. Titanium (IV) complex containing ONO-tridentate Schiff base ligand: Synthesis, crystal structure determination, Hirshfeld surface analysis, spectral characterization, theoretical and computational studies. *J. Mol. Struct.* **2021**, *1241*, No. 130653. (c) Ashfaq, M.; Munawar, K. S.; Tahir, M. N.; Dege, N.; Yaman, M.; Muhammad, S.; Alarfaji, S. S.; Kargar, H.; Arshad, M. U. Synthesis, Crystal Structure, Hirshfeld Surface Analysis, and Computational Study of a Novel Organic Salt Obtained from Benzylamine and an Acidic Component. *ACS Omega* **2021**, *6*, 22357−22366.
(32) (a) Raza, H.; Yildiz, I.; Yasmeen, F.; Munawar, K. S.; Ashfaq, M.; Abbas, M.; Ahmad, M.; Younus, H. A.; Zhang, S.; Ahmad, N. Synthesis of a 2D copper (II)-carboxylate framework having ultrafast adsorption of organic dyes. *J. Colloid Interface Sci.* **2021**, *602*, 43−54. (b) Kargar, H.; Fallah-Mehrjardi, M.; Behjatmanesh-Ardakani, R.; Tahir, M. N.; Ashfaq, M.; Munawar, K. S. Synthesis, crystal structure determination, Hirshfeld surface analysis, spectral characterization, theoretical and computational studies of titanium (IV) Schiff base complex. *J. Coord. Chem.* **2021**, *74*, 2682−2700. (c) Ali, A.; Kuznetsov, A.; Khan, M. U.; Tahir, M. N.; Ashfaq, M.; Raza; Muhammad, S. 2-Amino-6-methylpyridine based co-crystal salt formation using succinic acid: A.R.; Single-crystal analysis and computational exploration. *J. Mol. Struct.* **2021**, *1230*, No. 129893.
(33) Ashfaq, M.; Munawar, K. S.; Bogdanov, G.; Ali, A.; Tahir, M. N.; Ahmed, G.; Ramalingam, A.; Alam, M. M.; Imran, M.; Sambandam, S.; Munir, B. Single crystal inspection, Hirshfeld surface investigation and DFT study of a novel derivative of 4-fluoroaniline: 4-((4-fluorophenyl) amino)-4-oxobutanoic acid (BFAOB). *J. Iran. Chem. Soc.* **2021**, 1−9.
(34) Kargar, H.; Fallah-Mehrjardi, M.; Ashfaq, M.; Munawar, K. S.; Tahir, M. N.; Behjatmanesh-Ardakani, R.; Amiri Rudbari, H.; Adabi Ardakani, A.; Sedighi-Khavidak, S. Zn (II) complexes containing O, N, N, O-donor Schiff base ligands: synthesis, crystal structures, spectral investigations, biological activities, theoretical calculations and substitution effect on structures. *J. Coord. Chem.* **2021**, *74*, 2720−2740.
(35) (a) McKinnon, J. J.; Jayatilaka, D.; Spackman, M. A. Towards quantitative analysis of intermolecular interactions with Hirshfeld surfaces. *Commun. Chem.* **2007**, No. 3814. (b) Ashfaq, M.; Bogdanov, G.; Glebov, V.; Ali, A.; Tahir, M. N.; Abdullah, S. Single crystal investigation, Hirshfeld surface analysis and DFT exploration of the pyrimethamine-based novel organic salt: 2, 4-diamino-5-(4-chlorophenyl)-6-ethylpyrimidin-1-ium 3-carboxybenzoate hydrate (1: 1: 1). *J. Mol. Struct.* **2021**, *1224*, No. 129309. (c) Ashfaq, M.; Ali, A.; Kuznetsov, A.; Tahir, M. N.; Khalid, M. DFT and single-crystal investigation of the pyrimethamine-based novel co-crystal salt: 2, 4-diamino-5-(4-chlorophenyl)-6-ethylpyrimidin-1-ium-4-methylbenzoate hydrate (1: 1: 1)(DEMH). *J. Mol. Struct.* **2021**, *1228*, No. 129445.
(36) (a) Kargar, H.; Behjatmanesh-Ardakani, R.; Fallah-Mehrjardi, M.; Torabi, V.; Munawar, K. S.; Ashfaq, M.; Tahir, M. N. Ultrasound-based synthesis, SC-XRD, NMR, DFT, HSA of new Schiff bases derived from 2-aminopyridine: Experimental and theoretical studies. *J. Mol. Struct.* **2021**, *1233*, No. 130105. (b) Ashfaq, M.; Bogdanov, G.; Ali, A.; Tahir, M. N.; Abdullah, S. Pyrimethamine-Based Novel Co-Crystal Salt: Synthesis, Single-Crystal Investigation, Hirshfeld surface analysis and DFT inspection of the 2, 4-diamino-5-(4-chlorophenyl)-6-ethylpyrimidin-1-ium 2, 4-dichlorobenzoate (1: 1)(DECB). *J. Mol. Struct.* **2021**, *1235*, No. 130215. (c) Kargar, H.; Bazrafshan, M.; Fallah-Mehrjardi, M.; Behjatmanesh-Ardakani, R.; Rudbari, H. A.; Munawar, K. S.; Ashfaq, M.; Tahir, M. N. Synthesis, characterization, crystal structures, Hirshfeld surface analysis, DFT computational studies and catalytic activity of novel oxovanadium and dioxomolybdenum complexes with ONO tridentate Schiff base ligand. *Polyhedron* **2021**, *202*, No. 115194.
(37) Turner, M. J.; Grabowsky, S.; Jayatilaka, D.; Spackman, M. A. Accurate and efficient model energies for exploring intermolecular interactions in molecular crystals. *J. Phys. Chem. Lett.* **2014**, *5*, 4249−4255.
(38) Mackenzie, C. F.; Spackman, P. R.; Jayatilaka, D.; Spackman, M. A. CrystalExplorer model energies and energy frameworks: extension to metal coordination compounds, organic salts, solvates and open-shell systems. *IUCrJ* **2017**, *4*, 575−587.
(39) Frisch, M. J.; Trucks, G. W.; Schlegel, H. B.; Scuseria, G. E.; Robb, M. A.; Cheeseman, J. R.; Scalmani, G.; Barone, V.; Petersson, G. A.; Nakatsuji, H.; Li, X.; Caricato, M.; Marenich, A. V.; Bloino, J.; Janesko, B. G.; Gomperts, R.; Mennucci, B.; Hratchian, H. P.; Ortiz, J. V.; Izmaylov, A. F.; Sonnenberg, J. L.; Williams-Young, D.; Ding, F.; Lipparini, F.; Egidi, F.; Goings, J.; Peng, B.; Petrone, A.; Henderson, T.; Ranasinghe, D.; Zakrzewski, V. G.; Gao, J.; Rega, N.; Zheng, G.; Liang, W.; Hada, M.; Ehara, M.; Toyota, K.; Fukuda, R.; Hasegawa, J.; Ishida, M.; Nakajima, T.; Honda, Y.; Kitao, O.; Nakai, H.; Vreven, T.; Throssell, K.; Montgomery, J. A., Jr.; Peralta, J. E.; Ogliaro, F.; Bearpark, M. J.; Heyd, J. J.; Brothers, E. N.; Kudin, K. N.; Staroverov, V. N.; Keith, T. A.; Kobayashi, R.; Normand, J.; Raghavachari, K.; Rendell, A. P.; Burant, J. C.; Iyengar, S. S.; Tomasi, J.; Cossi, M.; Millam, J. M.; Klene, M.; Adamo, C.; Cammi,

https://doi.org/10.1021/acsomega.1c06325
ACS Omega 2022, 7, 5217−5230

R.; Ochterski, J. W.; Martin, R. L.; Morokuma, K.; Farkas, O.; Foresman, J. B.; Fox, D. J.. *Gaussian 16 Rev. B.01*; Gaussian, Inc.: Wallingford CT, 2016.
(40) Trott, O.; Olson, A. J. AutoDock Vina: improving the speed and accuracy of docking with a new scoring function, efficient optimization, and multithreading. *J. Comput. Chem.* **2010**, *31*, 455−461.
(41) Dallakyan, S. MGLTools, http://mgltools.scripps.edu/, 2010.
(42) Studio, D.. *Discovery Studio. Accelrys [2.1]*, 2008.
(43) (a) Zia, M.; Muhammad, S.; Bibi, S.; Abbasi, S. W.; Al-Sehemi, A. G.; Chaudhary, A. R.; Bai, F. Q. Exploring the potential of novel phenolic compounds as potential therapeutic candidates against SARS-CoV-2, using quantum chemistry, molecular docking and dynamic studies. *Bioorganic Med. Chem. Lett.* **2021**, *43*, No. 128079. (b) Muhammad, S.; Hassan, S. H.; Al-Sehemi, A. G.; Shakir, H. A.; Khan, M.; Irfan, M.; Iqbal, J. Exploring the new potential antiviral constituents of Moringa oliefera for SARS-COV-2 pathogenesis: An in silico molecular docking and dynamic studies. *Chem. Phys. Lett.* **2021**, *767*, No. 138379.
(44) Schuller, M.; Correy, G. J.; Gahbauer, S.; Fearon, D.; Wu, T.; Díaz, R. E.; Young, I. D.; Martins, L. C.; Smith, D. H.; Schulze-Gahmen, U.; Owens, T. W. Fragment binding to the Nsp3 macrodomain of SARS-CoV-2 identified through crystallographic screening and computational docking. *Sci. Adv.* **2021**, *7*, No. eabf8711.
(45) Kneller, D. W.; Phillips, G.; O'Neill, H. M.; Jedrzejczak, R.; Stols, L.; Langan, P.; Joachimiak, A.; Coates, L.; Kovalevsky, A. Structural plasticity of SARS-CoV-2 3CL M pro active site cavity revealed by room temperature X-ray crystallography. *Nat. Commun.* **2020**, *11*, No. 3202.
(46) Annunziata, G.; Sanduzzi Zamparelli, M.; Santoro, C.; Ciampaglia, R.; Stornaiuolo, M.; Tenore, G. C.; Sanduzzi, A.; Novellino, E. May polyphenols have a role against coronavirus infection? An overview of in vitro evidence. *Front. Med.* **2020**, *7*, No. 240.
(47) Burkhanova, T. M.; Babashkina, M. G.; Taskin-Tok, T.; Sharov, A. V.; Safin, D. A. Naphthalene-based bis-N-salicylidene aniline dyes: Crystal structures, Hirshfeld surface analysis, computational study and molecular docking with the SARS-CoV-2 proteins. *J. Iran. Chem. Soc.* **2021**, 1−13.
(48) Dahms, S. O.; Arciniega, M.; Steinmetzer, T.; Huber, R.; Than, M. E. Structure of the unliganded form of the proprotein convertase furin suggests activation by a substrate-induced mechanism. *Proc. Natl. Acad. Sci. U.S.A.* **2016**, *113*, 11196−11201.
(49) (a) Jawaria, R.; Khan, M. U.; Hussain, M.; Muhammad, S.; Sagir, M.; Hussain, A.; Al-Sehemi, A. G. Synthesis and characterization of ferrocene-based thiosemicarbazones along with their computational studies for potential as inhibitors for SARS-CoV-2. *J. Iran. Chem. Soc.* **2021**, 1−8. (b) Muhammad, S.; Hassan, S. H.; Al-Sehemi, A. G.; Shakir, H. A.; Khan, M.; Irfan, M.; Iqbal, J. Exploring the new potential antiviral constituents of Moringa oliefera for SARS-COV-2 pathogenesis: An in silico molecular docking and dynamic studies. *Chem. Phys. Lett.* **2021**, *767*, No. 138379.
(50) Bruker. *APEX2*; Bruker AXS Inc.: Madison, Wisconsin, USA, 2009.
(51) Sheldrick, G. M. A short history of SHELX. *Acta Crystallogr. A* **2008**, *64*, 112−122.
(52) Sheldrick, G. M. Crystal structure refinement with SHELXL. *Acta Crystallogr. C Struct. Chem.* **2015**, *71*, 3−8.
(53) Macrae, C. F.; Sovago, I.; Cottrell, S. J.; Galek, P. T.; McCabe, P.; Pidcock, E.; Platings, M.; Shields, G. P.; Stevens, J. S.; Towler, M.; Wood, P. A. Mercury 4.0: From visualization to analysis, design and prediction. *J. Appl. Crystallogr.* **2020**, *53*, 226−235.
(54) Spek, A. L. Structure validation in chemical crystallography. *Acta Crystallogr., Sect. D: Biol. Crystallogr.* **2009**, *65*, 148−155.

https://doi.org/10.1021/acsomega.1c06325
ACS Omega 2022, 7, 5217−5230